Chemical Vapor Deposition

DOI: 10.1002/cvde.200706671

Full Paper

Nanodiamond Tipped and Coated Conical Carbon Tubular Structures**

By *Boris Chernomordik, Santoshrupa Dumpala, Zhiqiang Q. Chen,* and *Mahendra K. Sunkara**

Studies of diamond nucleation and growth on conical carbon tubular structures show that the nucleation preferentially occurs at the tips, but only occurs on the sidewalls when they are pretreated with diamond or other powder dispersions, forming a nanodiamond coating. The high-resolution transmission electron microscopy (HRTEM) studies reveal that the diamond nucleation on the sidewalls may proceed through the formation of diamond nuclei within the walls at subsurface damage sites caused during pretreatment. In the case of experiments with low atomic hydrogen conditions, carbon onion structures are observed on the sidewalls but only with pretreatments.

Keywords: conical carbon, diamond, diamond nanotips, nucleation, onion, one-dimensional structures

1. Introduction

Conical carbon tubular morphologies such as carbon nanopipettes (CNP)[1] and tubular graphitic cones[2] represent a new morphological form for carbon nanotubes (CNTs) that taper from micrometer-scale bases to nanometer-scale tips. CNPs, with a high density of edge-plane sites on their surfaces, exhibit reversible behavior with redox reactions involving neurotransmitters, and also show promise for field emission.[3] The CNP arrays, due to the conical geometry of the individual structures, could easily be made into nanoelectrode ensembles.[4] Furthermore, the conical structures could serve as good templates for producing nanodiamond tip arrays, which could be made into diamond nanoelectrode ensembles easily by the simple polymer-masking technique described in our earlier work.[4] Also, the nanodiamond tip arrays could find interest in functionalized biosensor[5] and field emission[6] applications. Furthermore, there is an increased interest in synthesizing diamond-based, one-dimensional structures and their use in high-temperature diodes and composites.[7,8]

The conical carbon tubular structures are particularly interesting for studying diamond nucleation as their surfaces consist of a high density of edge-plane sites. Theoretical and experimental studies provided evidence that the nucleation may be mediated through hydrogenation of graphite edge-planes.[9–11] Recent experiments involving hydrogen exposure to multiwalled carbon nanotube (MWNT) structures yielded a high density of diamond nucleation throughout the MWNT while destroying the wall structures.[12] The same experiments performed over a longer duration resulted in the anisotropic growth of short diamond nanorods from the diamond crystals.[13] These studies suggest that the nucleation occurs via the formation of amorphous carbon.[14,15] In other studies using an external carbon source in a hot filament (HF)CVD reactor, single-walled (SW)CNTs were uniformly coated with nanodiamond.[16,17] In the case of diamond nucleation onto SWCNTs, it was proposed that the atomic hydrogen creates the necessary defect for subsequent hydrogenation to form nuclei for nanocrystalline diamond.[17] It was also reported that carbon can exist in body-centered cubic (bcc), face-centered cubic (fcc), and other phases at the nanometer scale[18] which may act as intermediates for diamond nucleation, although this has not been confirmed. Despite much progress through prior studies by a number of investigators, the pathway for diamond nucleation is not completely understood. In order to understand the nucleation process further, we investigated hydrogenation of the conical carbon tubular structures containing surfaces with a high density of edge-plane sites.

2. Results and Discussion

CNP arrays were synthesized onto platinum wire substrates that were immersed vertically in the microwave plasma, as shown schematically in Figure 1a. Diamond nucleation experiments were performed on horizontally placed CNP coated platinum wire substrates on a graphite

[*] Prof. M. K. Sunkara, B. Chernomordik, S. Dumpala
Department of Chemical Engineering, University of Louisville
Louisville, KY 40292 (USA)
E-mail: mahendra@louisville.edu
Dr. Z. Q. Chen
Institute for Advanced Materials and Renewable Energy,
University of Louisville
Louisville, KY 40292 (USA)

[**] The authors acknowledge financial support from the US Department of Energy (DE-FG02-05ER64071 and DE-FG02-07ER46375) B. Chernomordik acknowledges the financial support from the Barry M. Goldwater scholarship and the Grawemeyer Scholarship from the University of Louisville. Authors also acknowledge helpful discussions with Dr. Vidhya Chakrapani.

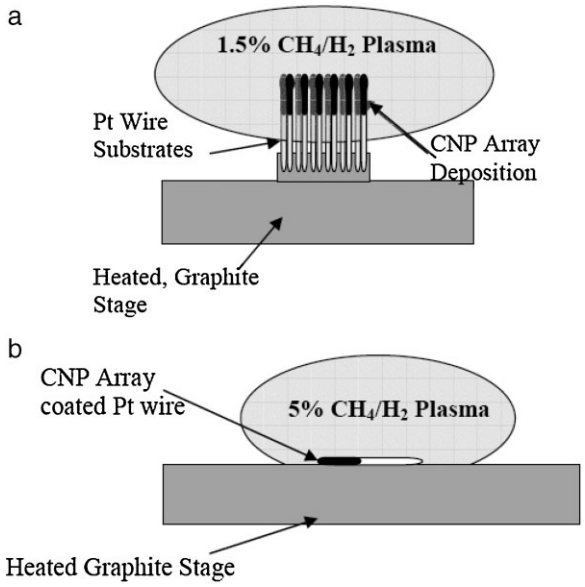

Fig. 1. a) A schematic illustrating the vertical positioning of the platinum wire substrates for the synthesis of CNPs. b) A schematic illustrating the horizontal positioning of the platinum wire substrates coated with CNP arrays for diamond nucleation and growth experiments.

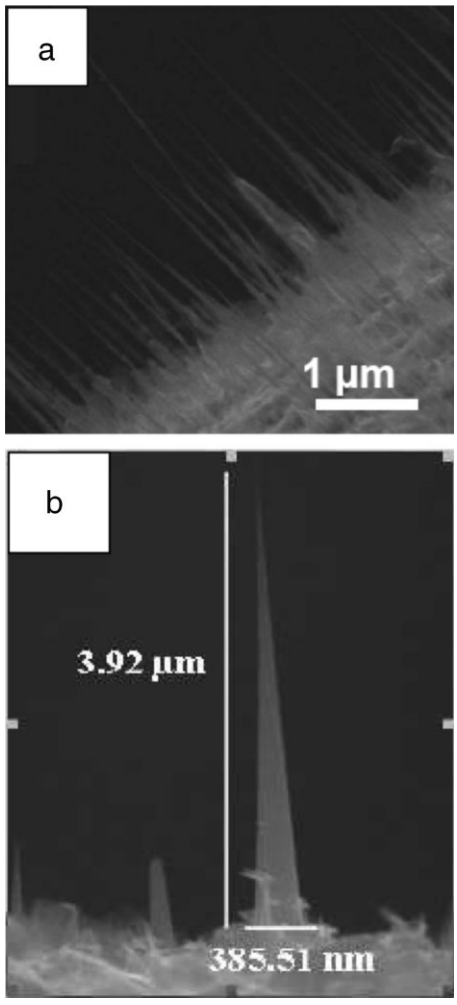

Fig. 2. SEM images of a) CNPs grown on bare platinum substrates, and b) an individual CNP structure.

susceptor in a microwave CVD reactor, as shown schematically in Figure 1b. Figure 2a shows the scanning electron microscope (SEM) images of the as-synthesized CNP arrays. Experiments showed that the aspect ratios and the array density vary with the substrate temperature, experimental duration, microwave power, and pressure. The diamond nucleation and growth experiments over short (20 min) durations on the as-synthesized CNP arrays resulted in selective nucleation and growth of sub-micrometer-size diamond crystals (200–500 nm in diameter) at their tips (see Fig. 3a). The diamond crystals were as large as 1.3 μm for experiments performed for about 3 h (Fig. 3b). For the diamond-tipped CNPs, Raman spectra (RS) were obtained using a 633 nm laser with a spot size of 1–2 μm over various sample regions. Figure 3d is a typical spectrum showing a peak at 1332 cm^{-1}, confirming that the crystals are diamond. Several observations were noted; firstly, the diamond crystals grew only at the tips of the CNPs, and secondly the CNP structures became straight CNTs with no appreciable change in their lengths. Both these observations are interesting and unexpected. In addition, the diamond crystals grown at the tips (as shown in Fig. 3c) seem to exhibit a high amount of rough faceting. Bright-field transmission electron microscope (TEM) images indicated that the rough faceting of the crystals is due to a high density of defective growth regions.

The rough faceting or high levels of defective growth observed for crystals growing on the tips of CNPs could probably be explained by a thermal runaway scenario. The temperature of the growing diamond crystal rises with increase in crystal size if the etched CNP cannot adequately support the transport of heat generated from the exothermic hydrogen recombination at the growing crystal surface.[19] A schematic of the model is shown in Figure 4a. A simple thermal transport model yields Equation 1.

$$\Delta T = \frac{J \cdot A_d \cdot \Delta H}{k \cdot A_t} \quad (1)$$

ΔT is the change in temperature, J is the hydrogen flux, A_d is the area of the diamond, ΔH is the total enthalpy, k is the thermal conductivity, and A_t is the cross-sectional area of the carbon nanotube. The heat of the recombination reaction, $H + H = H_2$, was taken as $\Delta H_r = -444$ kJ mol^{-1}.[20] The flux of hydrogen atom bombardment was calculated to be approximately 1×10^{-4} mol $cm^{-2} \cdot s^{-1}$, which is comparable to reported values.[20] A standard planar graphite conductivity value of 1000 W $m^{-1} \cdot K^{-1}$ was applied to a nanotube with a 20 nm OD and a 10 nm ID.[21] It can be

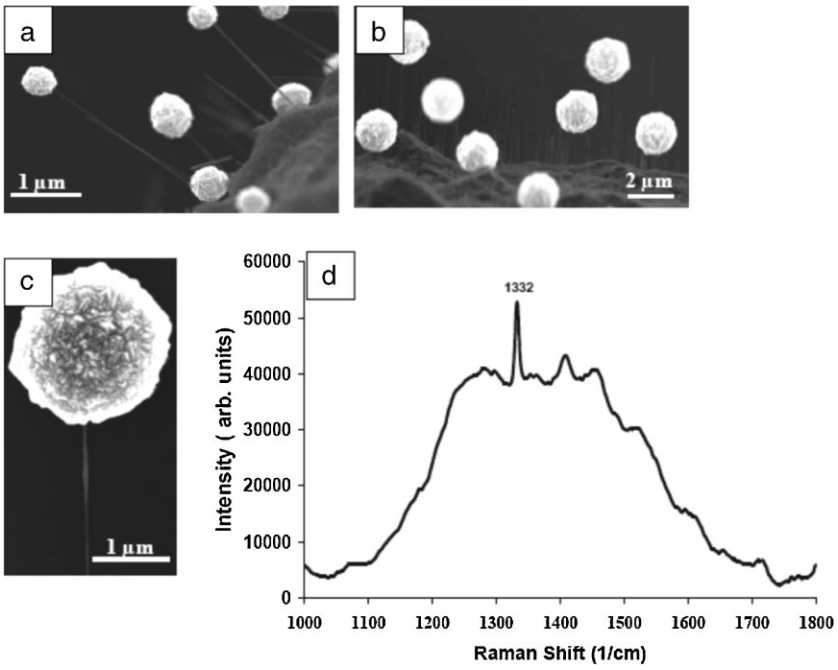

Fig. 3. SEM images of diamond growth on CNPs without pretreatment. a) Selective growth of sub-micrometer-scale crystals on the tips for ~20 min. b) Micrometer-scale diamond crystals grown for ~3 h. c) A diamond crystal (grown for ~3 h) at the tip of the straight carbon nanotube. d) Visible Raman spectra showing a peak at 1332 cm^{-1} corresponding to the diamond crystals at the tips of the CNPs shown in Fig. 3c.

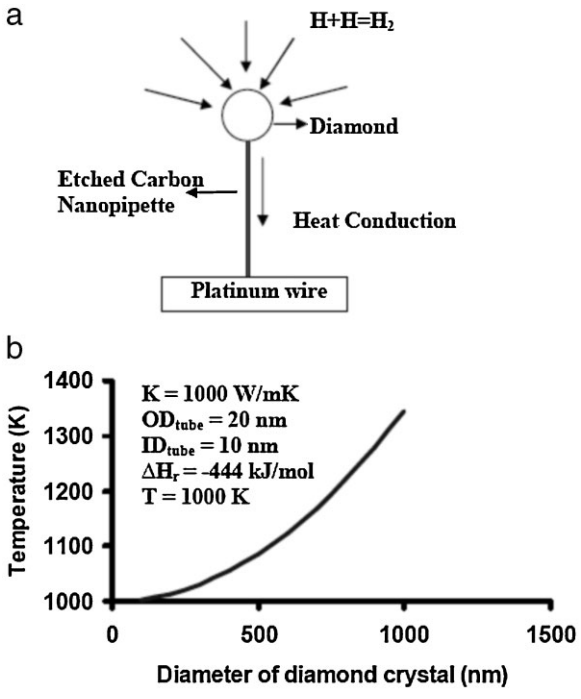

Fig. 4. a) A schematic illustrating the heat runaway scenario for a crystal growing at the tip of a thin CNT. b) A plot showing the estimated temperature rise during diamond growth as a function of diamond crystal size using the parameters indicated.

observed from Figure 4b that, as the diamond crystal increases in size, the temperature increases parabolically, leading to a runaway. Once heat build-up occurs, the temperature of the crystal rises, leading to defect generation which further roughens the crystal faceting.

The observation of preserved CNP lengths during etching is more surprising because the reactive atomic hydrogen should etch down the length of the CNP starting with the exposed graphitic edges at the tip.[9] The etching of these conical-shaped CNPs was further studied using hydrogen plasma exposure over short (20 min) durations. The etching of the conical CNP arrays shown in Figure 5a resulted in straight MWNTs with uniform diameter, as shown in Figure 5b. Figure 5b illustrates that all of the conical structures are converted into straight morphologies. Figure 5b also shows some intermittent results of etching where some CNPs are etched to different thicknesses along different lengths. Under these time scales (20 min) the lengths are preserved. High resolution (HR)TEM is used to understand the reasons for the preservation of lengths during etching by characterizing the structures at various stages of etching. Figures 5c and 5d show TEM images of the resulting straight multiwalled tubes. Furthermore, the insets in Figures 5c and 5d show lattice images which clearly indicate that the etching stops once the basal planes are exposed. These experiments confirmed that, during diamond growth, aggressive etching conditions exist at the CNP surface due to bombardment by hydrogen radicals. The HRTEM observations, presented in the inset of Figure 5e, showed closure of the graphene walls at the tip. The bright field image in Figure 5e shows a partially etched CNP with a closed tip, suggesting that closing of the tip happens simultaneously with the early stages of the etching process. As shown in Figure 5e, the etching, using atomic hydrogen, proceeds via formation of an amorphous hydrocarbon layer and subsequent removal of the amorphous layer eventually leading to straight tubes with only basal planes exposed, as shown in the inset of Figure 5d. Earlier theoretical calculations demonstrated that graphene sheets can curl up with hydrogenation, which can justify the closing of the CNP tips as observed during the diamond growth experiments.[10] On the other hand, there is no reasonable explanation for the observed selective nucleation of diamond crystals at the tips of conical carbon tubular structures. One possible explanation, however, is that the caps generated during closing of the tip could serve as preferential sites for diamond nucleation due to increased hydrogen absorption at the curved surfaces.[22]

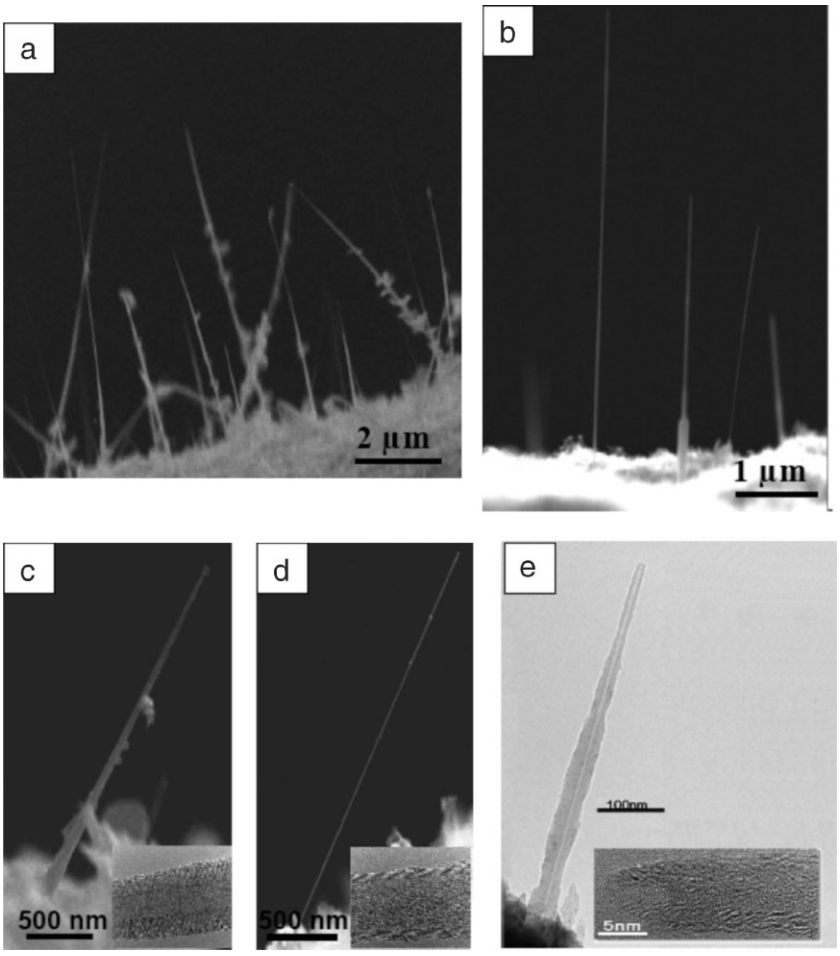

Fig. 5. a) SEM image of an array of as-synthesized CNPs with tapered morphology and various lengths before etching. b) SEM image of the CNP array shown in a) after etching using hydrogen plasma for 20 min. c) SEM image of a CNP showing the tapered structure with the inset showing the TEM image of the wall structure. d) SEM image of the CNP shown in c) after etching in hydrogen plasma for 20 min, while the inset shows a high resolution image of the etched tube. e) Bright field image of the partially etched CNP showing the closing of the tip, while the inset shows the HRTEM image of the tip.

The above experiments suggested that higher atomic hydrogen concentrations present harsher and more aggressive etching conditions, thus preventing nucleation on the outer surface of the CNP structures to form a nanocrystalline diamond coating. Experiments were conducted using electron cyclotron resonance (ECR) plasma under 50 mTorr with CNP samples which were pretreated by immersion in a sonicating diamond dispersion. Under these conditions, the etching of the CNP walls was minimal, preserving the conical morphology, as shown in Figure 6a, with small bright clusters on the CNP walls. Further examination of these structures using TEM revealed that the clusters were, in fact, carbon onion rings as shown in Figure 6b. The formation of carbon onions has been observed by other researchers during various processes such as electron-beam irradiation of carbon soot,[23] arc-discharge technique on carbon electrodes,[24] and an HFCVD process with continuous flow of carbon powder.[25] The present observations of carbon onion formation on the sidewalls of conical carbon tubes with pretreatment suggest that the defects induced on the sidewalls of the CNPs during pretreatment allow the formation of onions by curling of the walls in order to lower surface energy.[26,27] High resolution images of carbon onions, in Figure 6b, show the outward bending of the tube walls to form an onion structure, as illustrated in Figure 6c.

Transformation of carbon onions to diamond by exposure to an electron or ion-beam irradiation was reported in a number of studies. The nanometer-scale carbon onion centers were shown to provide nucleation sites for diamond when irradiated with a high intensity electron beam.[28] The carbon onions were suggested to mediate the transformation of CNTs to diamond with laser irradiation.[26] In addition, using the CNTs as heaters and carbon onions as high pressure cells, in situ observations of quasimelting of diamond and diamond-graphite transformations were recently achieved.[29] It is not clear, though, how and whether the carbon onion structures observed in the present study could serve as nucleation centers for diamond with further exposure to atomic hydrogen under CVD conditions.

Typically, diamond nucleation can be enhanced with pretreatments involving diamond powder dispersions. Two methods of pretreatment were used: immersion in a sonicating diamond dispersion, and electrophoretic seeding in a diamond powder bath. Diamond growth experiments using typical conditions were conducted on the pretreated CNP array substrates. The results are shown in Figure 7. Figure 7a shows an increased density of *selective* nucleation on the tips of CNPs when pretreated by just dipping in a sonication bath containing 0–2 μm commercial diamond powder for 20 s. The results were even more dramatic when the CNP arrays were treated by dipping in a sonication bath containing 0–250 nm nanodiamond powder. The results, as shown in Figure 7b, indicate nucleation and growth of nanocrystalline diamond occurs not only at the tips, but also along the length of CNPs. The CNP arrays were also pretreated using electrophoretic seeding with micrometer-scale and sub-micrometer-scale diamond powders. The resulting diamond nucleation densities are higher, as shown in Figures 7c–d. Figure 7e shows a typical UV Raman spectrum obtained using a 325 nm laser with a 1–2 μm spot size on the sample shown in Figure 7d,

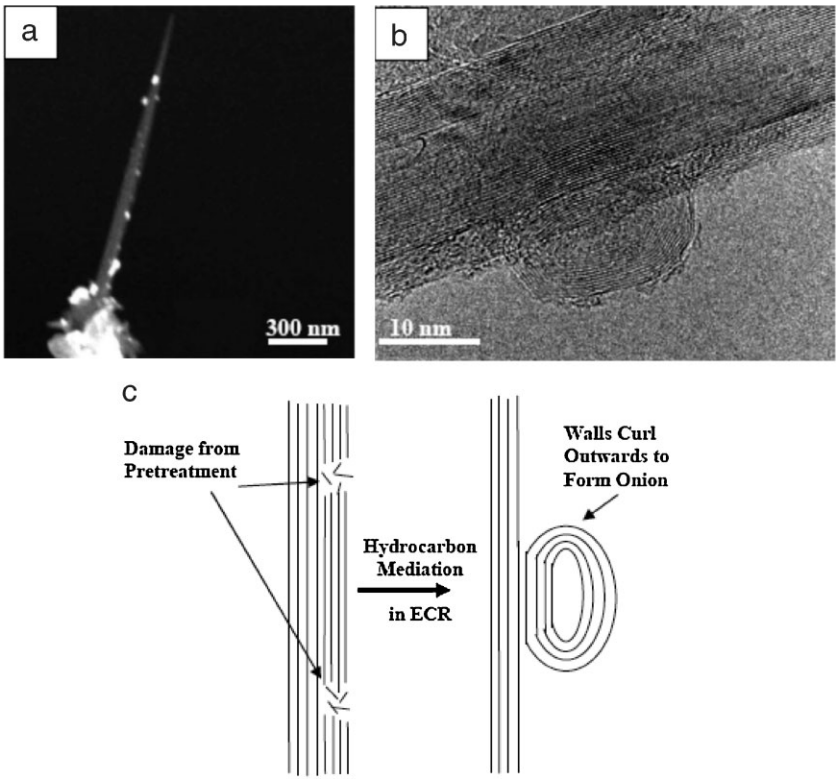

Fig. 6. a) A SEM image showing several bright clusters on the sidewall of CNPs. b) A high resolution image of one of the bright clusters indicating them to be a carbon onion. c) A schematic illustrating the curling mechanism of CNP walls at the damage sites, created during the pretreatment step.

which shows a peak at 1332 cm^{-1} confirming the presence of diamond crystals, as well as a peak at 1584 cm^{-1} characteristic of graphite. The nucleation density was highest on CNP arrays pretreated using electrophoretic seeding with submicrometer diamond powder, resulting in CNPs that were completely coated with a nanocrystalline diamond film. The use of smaller sized nanodiamond powders during electrophoretic seeding is expected to result in ultra-nanocrystalline diamond coating of CNPs. Experiments were also conducted in which CNPs were pretreated with boron carbide powder (0–7 μm). The results are similar to those treated using diamond powder, i.e., simple dipping into ultrasonic bath containing boron carbide powder resulted in an increased density of crystals at the CNP tips and electrophoretic seeding using boron carbide powder resulted in a high density of nucleation along the sidewalls, as shown in Figure 8. This is a significant result showing that nucleation onto the carbon tubular structures can be enhanced by pretreatments utilizing powders other than diamond, and the pretreatment powders *do not act like seeds*.

Short-term diamond growth experiments onto CNP arrays treated using either diamond powder or boron carbide powder dispersions show another interesting observation, i.e., the diamond crystals nucleate preferentially along the edges of the graphene planes rolling around the central nanotube.

The most interesting aspect of pretreatments is that both sonication and electrophoretic seeding significantly influenced the resulting diamond nucleation and growth on the wall structures of the CNPs. The reasons are not obvious, so the early stages of diamond nucleation on the walls of CNP structures were studied using HREM. Figures 9a and 9b show the diamond crystals originating within the inner tube walls of the CNP. The presence of both diamond and multiwalled graphite is supported by the indexed fast Fourier transform (FFT) pattern of the HREM image shown in the inset of Figure 9b. The forbidden (020) reflection is seen in the FFT pattern in Figure 9b. This may be due to kinematic effects in crystals with thicknesses greater than 10 nm, or in a crystal that has fcc or ''n-diamond'' phase.[18] As the crystal seen here is about 10 nm or larger, it is probably due to thickness effect rather than the crystal being fcc carbon phase. The FFT reconstruction from the diffraction maxima corresponding to a diamond-cubic structure is shown in Figure 9c. The FFT reconstruction from the diffraction bands corresponding to multiple graphene walls is shown in Figure 9d. These results confirm that the core diamond crystal is surrounded by multigraphene walls. The energy loss near edge structure (ELNES) in Figure 9e for carbon-K presents π^* and σ^* edges. Generally, the ELNES of C-K edge in diamond has σ^* peaks, whereas for graphene there is only a π^* peak.[15,30] In our spectrum of the edge of nanodiamond crystal, both π^* and sharp σ^* peaks are evident, thus showing that the nanodiamond crystallites on the CNP walls are surrounded by multigraphene walls.

Based on all the above observations, a possible mechanism is proposed for the nucleation of diamond with pretreatment. 1) The impacts by seed particles during pretreatment damage the wall structure of the CNPs introducing subsurface defects. 2) Hydrogenation of the subsurface defects forms an amorphous hydrogenated carbon phase. 3) Subsequent slow hydrogenation of the amorphous carbon phase regions leads to the nucleation of diamond, whereas nucleation on the outer walls is prevented due to the aggressive etching conditions. It had been previously reported that defects on CNT walls serve as sites for diamond nucleation through formation of an amorphous carbon phase.[12,17] Diamond nucleation through transition from amorphous carbon has also been described on non-carbon substrates.[14,15] More experiments and HRTEM

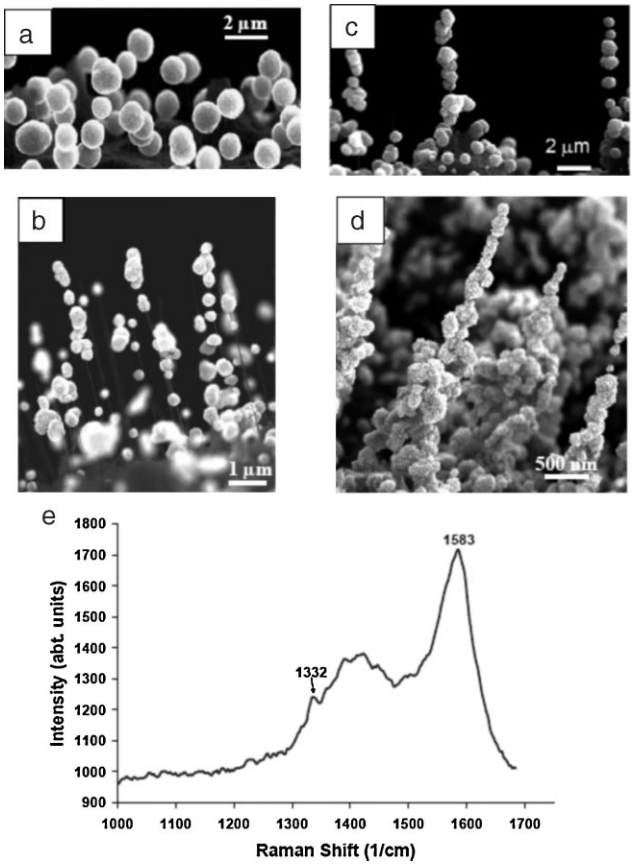

Fig. 7. SEM images showing diamond nucleation and growth on CNPs after pretreatment using the sonic bath dispersions of: a) micrometer-scale diamond powder; and b) sub-micrometer-scale diamond powder. Results of pretreatment using electrophoretic seeding in dispersions of: c) micrometer-scale diamond powder; and d) sub-micrometer-scale diamond powder. e) A UV Raman spectrograph confirming the presence of diamond with a peak at 1332 cm^{-1}.

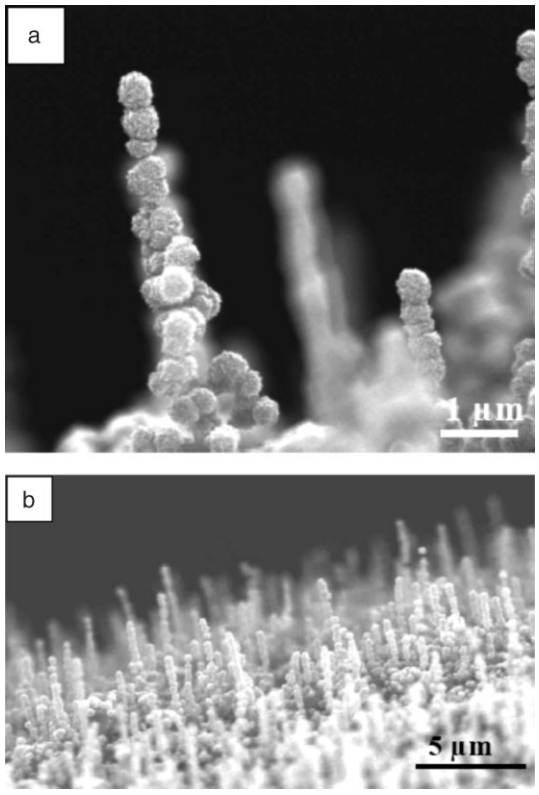

Fig. 8. SEM images showing CNPs treated with boron carbide powder. a) Shows the complete coating of diamond crystals along the length of a CNP clearly depicting the spiral growth of diamond crystals. b) Shows a large array of CNPs coated with diamond crystals.

studies are needed to understand which mechanism is the most likely one. Nevertheless, the above results may provide an insight into the essential reasons for enhanced nucleation with impacts from diamond powders.

3. Conclusions

This study reports diamond nucleation experiments on conical CNP structures. Diamond nucleation onto untreated CNP arrays occurred selectively at the tips while etching the rest of the CNP body, transforming it into a thin, straight CNT while preserving the length. Pretreatments using either diamond or boron carbide powder dispersions improved the nucleation density on the tips and also on the sidewalls, forming a nanocrystalline diamond coating on the CNPs. The early stage diamond nucleation experiments over short durations involving pretreated CNPs indicate that the nucleation of diamond crystals occurs within the walls (or sub-surface) of CNT structures. Experiments using low-pressure hydrogen plasma in ECR resulted in the nucleation of carbon onions on the sidewalls of CNPs. Based on all the observations, a likely mechanism is proposed to explain the role of pretreatment, i.e., the slow hydrogenation kinetics at subsurface defects created during pretreatments leads to diamond nuclei formation inside the walls of MWNTs or conical CNT structures.

4. Experimental

The CNP arrays were synthesized using platinum wire substrates placed vertically into microwave plasma in an ASTeX model 5010 microwave plasma-enhanced (MPE)CVD reactor. The synthesis experiments were conducted using 1.5% CH_4 in H_2 (200 sccm H_2) and using microwave power of 950 W under a pressure of 20–25 Torr for at least 3 h.

Diamond nucleation and growth experiments were performed by placing the CNP-coated platinum wire substrates horizontally onto a graphite susceptor in a SEKI model AX5200S-ECR MWCVD reactor equipped with an RF-induction heated stage. Several experiments were conducted using a methane composition ranging from 2–5% in hydrogen (200 sccm H_2) using MW power of 900 W and substrate temperature of 1023 K under 25 Torr pressure.

Using a SEKI model AX5200S-ECR MWCVD reactor, some other experiments were conducted on CNP array-coated platinum wire substrates using ECR plasma at pressures ranging from 50–100 mTorr with methane composition ranging from 0–5% CH_4 in H_2 using 500 Watts of MW power and

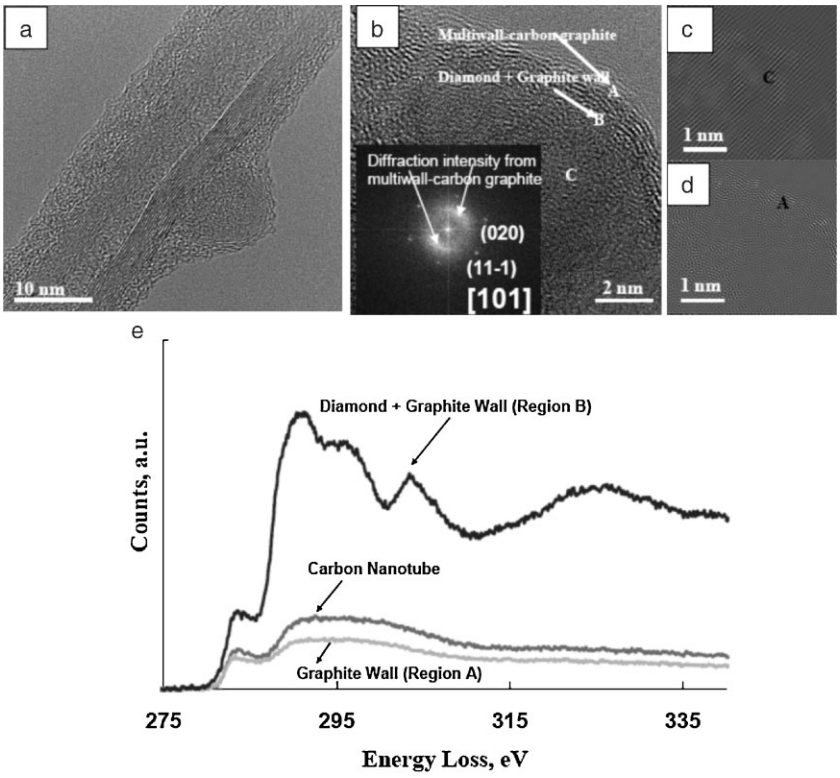

Fig. 9. a) HTREM image of a diamond crystal nucleated within the subsurface layer. b) A subsurface diamond crystal is shown with regions labeled as 'A' for tube walls, 'B' for the region between diamond and tube wall, and 'C' for the inner diamond crystal. The inset is an FFT pattern showing the diffraction bands and maxima resulting from both MWNT and diamond, respectively. c) FFT reconstructed image from the maxima corresponding to diamond from region 'C', and d) FFT reconstructed image from the diffraction corresponding to the multiwall graphite from region 'A'. e) ELNES of carbon-K edge showing a mixture of diamond and MWNT.

a substrate temperature of 1000 K for 2 h. The samples were primarily analyzed using a field-emission SEM (FEI Model Nova600 nanoSEM) and a 200 keV TECNAI F20 TEM with a Gatan 2002 GIF system.

Received: November 29, 2007
Revised: February 20, 2008

[1] R. C. Mani, X. Li, M. K. Sunkara, K. Rajan, *Nano Lett.* **2003**, *3*, 671.
[2] G. Zhang, X. Jiang, E. Wang, *Science* **2003**, *300*, 472.
[3] J. J. Li, C. Z. Gu, Q. Wang, P. Xu, Z. L. Wang, Z. Xu, X. D. Ba, *Appl. Phys. Lett.* **2005**, *87*, 143107.
[4] R. D. Lowe, R. C. Mani, R. P. Baldwin, M. K. Sunakra, *Electrochem. Solid State Lett.* **2006**, *9*, H43.
[5] P. H. Chung, E. Perevedentseva, J. S. Tu, C. C. Chang, C. L. Cheng, *Diamond Relat. Mater.* **2006**, *15*, 622.
[6] K. Subramanian, W. P. Kang, J. L. Davidson, W. H. Hofmeister, B. K. Choi, M. Howell, *Diamond Relat. Mater.* **2006**, *14*, **2099.**
[7] R. Arenal, P. Bruno, D. J. Miller, M. Bleuel, J. Lal, D. M. Gruen, *Phys. Rev. B* **2007**, *75*, 195431.
[8] I. I. Vlasov, O. I. Lebedev, V. G. Ralchenko, E. Goovaerts, G. Bertoni, G. Van Tendeloo, V. I. Konov, *Adv. Mater.* **2007**, *19*, 4058.
[9] W. R. L. Lambrecht, C. H. Lee, B. Segall, J. C. Angus, Z. Li, M. Sunkara, *Nature* **1993**, *364*, 607.
[10] S. P. Mehandru, A. B. Anderson, J. C. Angus, *J. Phys. Chem.* **1992**, *96*, 10978.
[11] Z. Li, L. Wang, T. Suzuki, P. Pirouz, J. C. Angus, *J. Appl. Phys.* **1993**, *73*, 711.
[12] L. T. Sun, J. L. Gong, Z. Y. Zhu, S. X. He, Z. X. Wang, *App. Phys. Lett.* **2004**, *84*, 2901.
[13] L. T. Sun, J. Gong, D. Zhu, Z. Zhu, S. He, *Adv. Mater.* **2004**, *16*, 1849.
[14] Y. Lifshitz, T. Köhler, T. Frauenheim, I. Guzmann, A. Hoffman, R. Q. Zhang, X. T. Zhou, S. T. Lee, *Science* **2002**, *297*, 1531.
[15] Y. Lifshitz, X. M. Meng, S. T. Lee, R. Akhveldiany, A. Hoffman, *Phys. Rev. Lett.* **2004**, *93*, 056101-1.
[16] M. L. Terranova, S. Orlanducci, A. Fiori, E. Tamburri, V. Sessa, M. Rossi, A. S. Barnard, *Chem. Mater.* **2005**, *17*, 3214.
[17] A. S. Barnard, M. L. Terranova, M. Rossi, *Chem. Mater.* **2005**, *17*, 527.
[18] J. Cowley, R. C. Mani, M. K. Sunkara, M. O'Keeffe, C. Bonneau, *Chem. Mater.* **2004**, *16*, 4905.
[19] R. Gat, J. C. Angus, *J. Appl. Phys.* **1993**, *74*, 5981.
[20] C. Wolden, S. Mitra, K. K. Gleason, *J. Appl. Phys.* **1992**, *72*, 3750.
[21] J. Che, T. Cagin, W. A. Goddard III, *Nanotechnol.* **2000**, *11*, 65.
[22] P. Ruffieux, O. Gröning, M. Bielmann, P. Mauron, L. Schalpbach, P. Gröning, *Phys. Rev. B.* **2002**, *66*, 245416.
[23] D. Ugarte, *Nature* **1992**, *359*, 707.
[24] N. Sano, H. Wang, I. Alexandrou, M. Chhowalla, K. B. K. Teo, G. A. J. Amaratunga, *J. Appl. Phys.* **2002**, *92*, 2783.
[25] S. Orlanducci, A. Fiori, E. Tamburri, V. Sessa, M. L. Terranova, M. Rossi, *Cryst. Res. Technol.* **2005**, *40*, 928.
[26] D. H. Robertson, D. W. Brenner, C. T. White, *J. Phys. Chem.* **1992**, *96*, 6133.
[27] B. Wei, J. Zhang, J. Liang, D. Wv, *Carbon* **1998**, *36*, 997.
[28] F. Banhart, P. M. Ajayan, *Nature* **1996**, *382*, 433.
[29] J. Y. Huang, *Nano Lett.* **2007**, *7*, 2335.
[30] A. L. Hamon, J. Verbeeck, D. Schryvers, J. Benedikt, R. M. C. M. Van der Sanden, *J. Mater. Chem.* **2004**, *14*, 2030.

